# QSO ABSORPTION LINES AS CHRONICLE OF THE STRUCTURE FORMATION HISTORY

J.P. MÜCKET, R. RIEDIGER
*Astrophysikalisches Institut Potsdam, An der Sternwarte 16, D 14482 Potsdam, Germany*

P. PETITJEAN
*Institut d'Astrophysique de Paris, CNRS, 98bis Boulevard Arago, F 75014 Paris, France*

We study the evolution of the Lyman$\alpha$ forest from redshift $z \approx 5$ to $z = 0$, in a CDM model using numerical simulations including collisionless particles only. The baryonic component is assumed to follow the dark matter distribution. The separate contributions of clouds mainly located in voids and of clouds associated with dense structures (filaments) to the characteristics of the Lyman$\alpha$ forest (dn/dz, dn/dN(HI) etc.) are examined. We are able to make predictions for the number density of lines per unit redshift at $z = 0$.

Over the past half decade considerable progress has been made in the theoretical understanding of the nature of the Lyman$\alpha$ forest. The common outcome of related investigations (Cen et al. [3], Petitjean et al. [12], Mücket et al. [10], Hernquist et al. [4], Miralda-Escudé et al. [9], Zhang et al. [15] is the interpretation of the Lyman$\alpha$ absorption as originated by an inhomogeneous IGM pervaded by a background ionizing radiation field. The latter is probably originated by QSOs and/or star-forming galaxies. In all recent models a direct relation between the Lyman$\alpha$ forest and the cosmological structure formation is presumed. Since the results obtained from the simulations agree with the corresponding quantities from observations quantitatively it could be expected that further investigations could lead to new constraints with respect to the underlying cosmological models. Since observational data are available now at almost all redshifts up to z=5 one would wish to model the complete lines of sight in order to link the Lyman$\alpha$ forest evolution at high and low redshifts to the cosmic structure formation during the epoch $0 < z < 5$. The hydro-simulations are already able to give a very detailed description of the Lyman$\alpha$ forest. The amount of computing time is such however that most of the descriptions are limited to $z > 2$. Using assumptions that have been shown to be valid in the low density regime we study the evolution of the Lyman$\alpha$ forest over the whole redshift range $0 \leq z < 5$. Our assumption that the Lyman$\alpha$ gas traces the shallower potential wells of the dark matter distribution (i.e. $\Omega_b$ is assumed to be constant all the time) allows for using numerical simu-

lations including collisionless particles only. Thus the needed computational time can be decreased considerably. This approximation has been shown to be valid for the low-density regime characteristic of the Lyman$\alpha$ forest by detailed hydro-simulations (see Miralda-Escudé et al.[9], Hernquist[4], Yepes et al.[14], and also Hui et al.[6]). The details of our simulation, especially how an appropriate description of the thermodynamic quantities and their evolution has been incorporated into the particle code, is given in Mücket et. al[10].

The intensity of the photo-ionizing UV background flux, assumed to be homogeneous and isotropic inside the simulation box, is computed in the course of the simulation. The variation of the flux is assumed to be related to the amount of cooled gas that collapses at any given time.

We distinguish between particles for which shock heating is important enough to significantly increase the gas temperature above the temperature resulting from photo-ionization (population $P_{\rm s}$) and the remainder of the particles (population $P_{\rm u}$). Population $P_{\rm s}$ particles are mostly found in big halos and elongated filamentary structures (regions of enhanced density). The population $P_{\rm u}$ is present in the surroundings of the structures formed by shocked particles but mostly in the voids delineated by these structures. The fraction of particles belonging to population $P_{\rm u}$ is changing with time: 77% at $z = 3$, 67% at $z = 2$, 40% at $z = 0.5$ and 25% at $z = 0$.

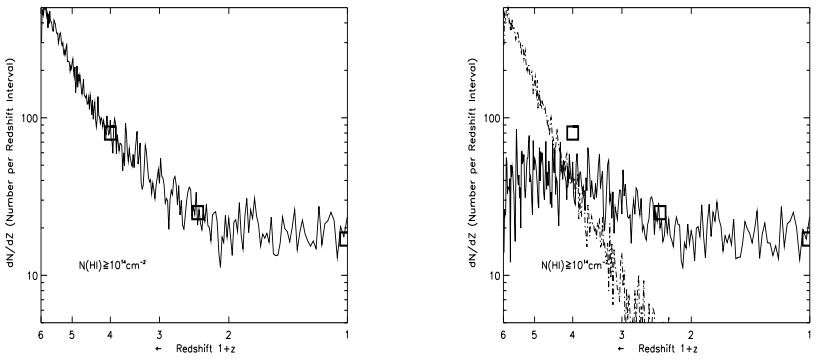


Figure 1: a) Number density $\mathrm{d}n/\mathrm{d}z$ of clouds with column density $\log N(\mathrm{HI}) > 14$ versus redshift $z$; b) As in a) the number density of lines drawn from populations $P_{\rm s}$ and $P_{\rm u}$ are plotted as full and dash-dotted lines respectively

We use the simulation to synthesize spectra along a line of sight to a fictitious QSO at $z = 5$ (see also Riediger et al.[13]). A first test of the model is that the evolution of the average Lyman$\alpha$ decrement should be reproduced.

The comparison of the computed flux decrement evolution with the observational data has been used for normalizing the flux. A value of $J_{-21}(z_0) = 0.1$ at $z_0 \sim 3$ fits the decrement evolution quite well .

An important quantity to be compared with observations is the number density per unit redshift interval and its time-dependent behavior. It can be seen from Fig. 1a that the evolution of the total number of strong lines is well reproduced. Data are taken from Lu et al. [7], Petitjean et al. [11] and Bahcall [1]. If the number of lines per unit redshift is approximated by a power-law, $\mathrm{d}n/\mathrm{d}z \propto (1+z)^{\gamma}$, we find $\gamma \approx 2.6$ for $1.5 < z < 3$ and $\gamma \approx 0.6$ for $0 < z < 1.5$ (after smoothing). However the slope of $\mathrm{d}n/\mathrm{d}z$ steepens at $z > 3$. Fitting the number density evolution for $1.5 < z < 5$ by a single power law we get $\gamma \approx 2.9$.

Fig. 1b shows the contributions of the two populations of clouds with $N(\mathrm{HI}) > 10^{14}$ cm$^{-2}$, $P_{\mathrm{s}}$ (solid line) and $P_{\mathrm{u}}$ (dash-dotted line). It is apparent that the dominant population is different before and after $z \sim 3$. At high redshift, most of the lines arise in $P_{\mathrm{u}}$ particles whereas at low redshift, most of the gas is condensed in filamentary structures (see Petitjean et al. [12]). The very steep slope found for the number density evolution of the $P_{\mathrm{u}}$ clouds as shown in Fig. 1b is mainly due to decreasing HI column densities through individual clouds.

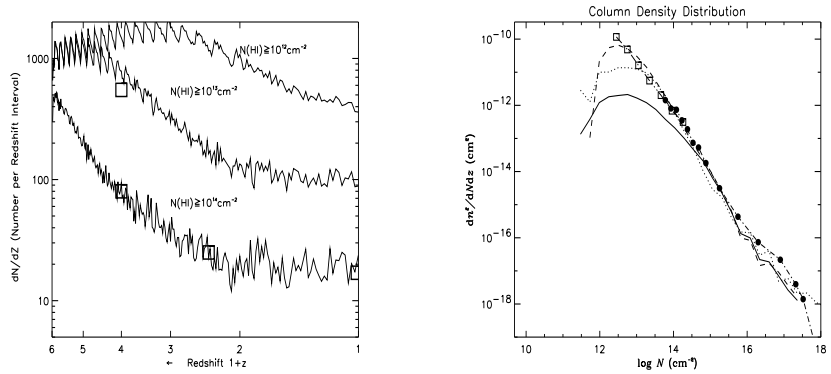


Figure 2: a) Number density of lines versus redshift for different column density thresholds $\log N(HI) > 12, 13, 14$; b) $HI$ column density distribution at $z = 3$ computed directly from the simulation (dashed line), after reanalysing a sample of computed spectra (dotted line), and for population $P_s$ only (solid line). Observational ponts: Hu et al. [5] (squares), Petitjean et al. [11] (filled circles).

The number density of lines with $N(\mathrm{HI}) > 10^{12}$ cm$^{-2}$ is about constant over the redshift range $1 < z < 5$ (see Fig. 2a) and decreases slowly at lower redshift.

Low density gas is found in regions delineated by filamentary structures at high redshift. This gas slowly disappears. The total number density of lines stays nearly constant because the high column density gas has column density decreasing with time. This difference in the evolution of the number density of weak and strong lines has been noticed in intermediate resolution data (Bechtold [2]) and confirmed by Kim et al. [8]. The latter authors find $\gamma = 2.41 \pm 0.18$ and $1.29 \pm 0.45$ for $\log N(\mathrm{HI}) > 10^{14}$ and $10^{13}$ cm$^{-2}$ respectively.

The resulting column density distribution shown in Fig. 2b determined from the simulated spectra show a remarkable agreement with the observations.

The number density of lines per unit redshift at $z \sim 0$ with column densities $\log N(\mathrm{HI}) > 12, 13, 14$ is expected to be 400, 100, and 20 respectively. At low redshift, if most of the strong ($w_\mathrm{r} > 0.3$ Å) lines are associated with galaxies, the bulk of the Lyman$\alpha$ forest however should have lower equivalent width and should not be tightly correlated with galaxies. Our model predicts that the number of weak lines should be large at low redshift and gives therefore an interesting test of the overall picture. This prediction can be tested along the line of sight to 3C273 with the new instrumentation on the Hubble Space Telescope.

## References


1. J.N. Bahcall, J. Bergeron, A. Boksenberg, et al., *ApJS* **87**, 1 (1993)
2. J. Bechtold, *ApJS* **91**, 1 (1994)
3. R. Cen, J. Miralda-Escudé, J.P. Ostriker, M. Rauch, *ApJL* **437**, L9 (1994)
4. L. Hernquist, N. Katz, D.H. Weinberg,et al., 1996, *ApJ* **457**, L51 (1996)
5. E.M. Hu, T.-S. Kim, L.L. Cowie, A. Songaila, M. Rauch, *AJ* **110**, 1526 (1995)
6. L. Hui, N.Y. Gnedin, Y. Zhang, astro-ph/9702167, 1997
7. L. Lu, A.M. Wolfe, D.A. Turnshek, *ApJ* **367**, 19 (1991)
8. T.-S. Kim, E.M. Hu, L.L. Cowe, A. Songaila, astro-ph/9704184, (1997)
9. J. Miralda-Escudeé, R. Cen, J.P. Ostriker, M. Rauch, 1996, *ApJ* **471**, 582 (1996)
10. J.P. Mücket, P. Petitjean, R. Kates, R. Riediger, *Astron.Astrophys.* **308**, 17 (1996)
11. P. Petitjean, J.K. Webb, M. Rauch, et al.; *MNRAS* **262**, 499 (1993)
12. P. Petitjean, J.P. Mücket, R.E. Kates, *Astron.Astrophys.* **295**, L9 (1995)
13. R. Riediger, P. Petitjean, J.P. Mücket, *Astron.Astrophys.*, in press (1993)
14. G. Yepes, R. Kates, A. Khokhlov, A. Klypin, *MNRAS* **284**, 235 (1997)
15. Y. Zhang, A. Meiksin, P. Anninos, M.L. Norman, astro-ph/9609194, 1996